ORIGINAL ARTICLE

A novel investigation into the edge effect reduction of 4340 steel disc through induction hardening process using magnetic flux concentrators

Mahyar Parvinzadeh [1] · Sasan Sattarpanah Karganroudi [1] · Narges Omidi [1] · Noureddine Barka [1] · Mohamed Khalifa [1]

Abstract
Induction hardening serves as one of the best mass production processes used recently due to its ability to quickly generate high-intensity heat in a well-defined location of the part. Numerous advantages of this method make it a reliable technique to produce a thin martensite layer on the part surface that has compressive residual stresses. In this regard, the presented study is devoted to investigating utilizing induction heating for surface hardening of AISI 4340 steel disc. The purpose is to evaluate the performance of magnetic flux concentrators and the effects of the induction process parameter on the case-depth and edge effect in the surface hardening of the disc. Once the proper range of parameters is defined, Taguchi experimentation planning is used to frame comprehensive experimentation with the minimum possible trial. Then, the case-depth of discs is evaluated on their cross-sections (edge and middle plane) through hardness profile measurement of samples using a micro-indentation hardness machine. The results are then statistically analyzed using analysis of variance (ANOVA) and response surface methodology (RSM) to determine the best combination of parameters to achieve maximum case-depth yet minimum edge effect. The goodness-of-fit regression models are then developed to predict the case-depth profile as a function of machine parameters based on linear regression utilizing case-depth responses in the edge and middle planes of discs. Results imply that maximum case-depth with minimum edge effect can be produced by using the highest heating time along with the average amplitude of the power, axial gap, and radial gap. This study gives a good exploration of case-depths optimized by setting up process parameters when a magnetic flux concentrator is utilized; thus, a guideline to reduce discs edge effect in induction surface hardening application is given.

1 Introduction

The importance of induction heat treatment and its numerous applications have been increased over the last decades. One of the most sought-after usages of this phenomenon is the hardening of metals [1, 2]. Multiple advantages of induction heat treatment make it superior to traditional methods: capability to produce high power density in a shorter time that results in saving time, being high energy efficient, limiting the risks of distortion and deformation during conventional heat treatments [3]. It is a fast and clean-energy process and repeatable

in terms of treating parts with the same quality. Also, the ability of fast heat generation in well-defined points of the specimen and eliminating other undesired-treated parts, being environmental-friendly along with other mentioned characteristics, makes this method well-received for mass production and industrial purposes [4]. The ability to generate localized heat during the heating process in hardening processes is one of the most important industrial applications of induction heating employing improving wear and fatigue resistance of the parts such as bearings, shafts, and disc-shaped parts like gears [5, 6].

Parts geometry, surface topology, chemical composition, and induction heating processing parameters are crucial elements in induction surface hardening [7]. This study aims at investigating the effects of induction machine parameters on parts with plain geometry like a disc. While the result of this simplification can be generalized to gears [8], considering

✉ Sasan Sattarpanah Karganroudi
sasan_sattarpanahkarganroudi@uqar.ca

1 Department of Mathematics, Computer Science and Engineering, Université du Québec à Rimouski, Rimouski, Quebec, Canada

simpler geometries like disc rather than gear can eliminate some redundant parameters which are related to gear-shaped parts and geometrical complications (Fig. 1).

Similar to conventional hardening methods, the induction hardening process is based on increasing the temperature up to the austenitic area, then cooling the part rapidly. As a result, the martensite phase, a very hard steel structure, is formed. However, the hardenability of the metal alloy plays a key role in the final percentage of the martensite phase. In this study, AISI 4340 steel, which is known for its heat treatable properties, is used to achieve high strength, good fatigue resistance, and proper atmospheric corrosion resistance behaviors. Referring to the main goal of the study, obtaining a hard surface on 4340 steel discs, creating maximum martensite in surface layers is intended since the formation of any pearlite or bainite phase causes a drop in the hardness of the material. To eliminate producing pearlite or bainite formation, rapid quenching of a uniform austenite layer is essential [9]. A desirable form of austenite layer highly depends on induction process parameters that could maximize the austenite phase formation. The subsequent step of quenching is done by a water shower to create a uniform martensitic layer on the parts' surface. According to these facts, a typical heat treatment temperature for AISI 4340 alloy steel parts is within a range of 790 to 915 °C (850 °C in our study) to create a uniform austenite layer, and a rapid quenching to produce the maximum possible percentage of martensite layer [10–13].

Despite the brilliant advantages of induction hardening, the process yet involves some challenges that lead to undesirable results. The major issue in induction heat treatment is the edge effect due to the disproportionate density of magnetic flux in different areas of a part [4, 14]. This variation causes non-uniform generated temperatures over the surface of parts. Subsequently, an uneven formation of martensite phases will occur on the surface of the specimen following the quenching may lead to undesirable metallographic structure. These physical phenomena arising from magnetic flux characteristics coupled wi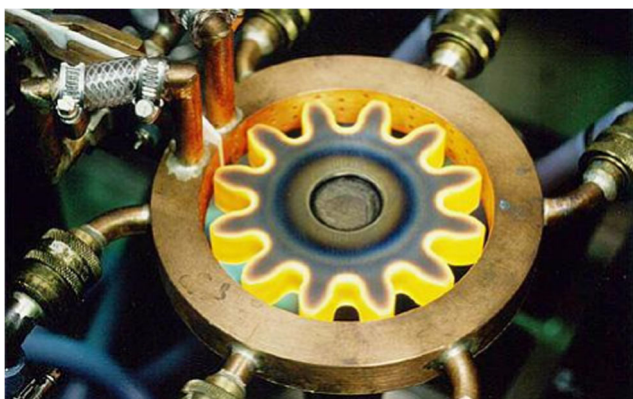th coil geometry limitation provide a varying temperature distribution in radial and axial directions. In the case of high-frequency induction hardening of a small disc with a single-shot method, two facts could be concluded to justify the non-uniform temperature distribution: First, the temperature gradient in the radial direction due to the more proximity in the outer layer of the disc to the induction coil compared with the distant layer to the coil toward the center of the disc's geometry. The second reason for nonuniform temperature distribution comes from the distortion of magnetic field at coil and bending of the induced current in the edge regions of the workpiece, namely, the edge effect phenomenon. This results in a temperature gradient in the axial direction wherein the generated heat profile between the middle plate and side plates of a disc is not uniform as shown in Fig. 2. Thermal gradient because of the edge effect is negligible for big parts, though this is not applicable for small parts. The smaller the workpiece, the more serious challenge in the quality of the final product [15–17]. Due to the complexity of this physical phenomenon, there is no definite solution to eliminate it; however, a great deal of researches has been dedicated to reducing its consequences as much as possible. One efficient solution is to utilize magnetic flux concentrators. Axial/radial gaps between magnetic flux concentrators and coil/disc are two effective parameters in the edge effect that are included in this study. This study investigates the effect of the concentrators position (radial and axial gap) as well as the induction heating process parameters including machine power, frequency, and heating time on the edge effect aiming at tuning them to minimize the edge effect. Figure 3 demonstrates a schematic presentation of the position of the coil, concentrator, and workpiece.
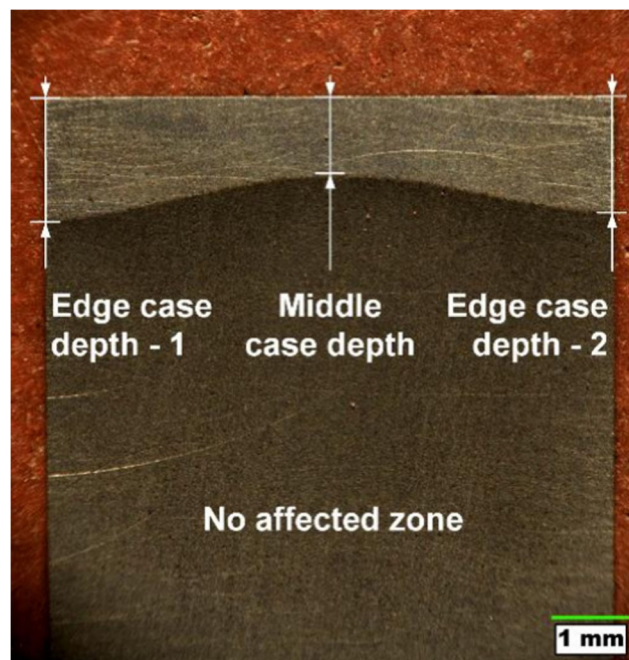

Fig. 1 Induction hardening of the gear [8]

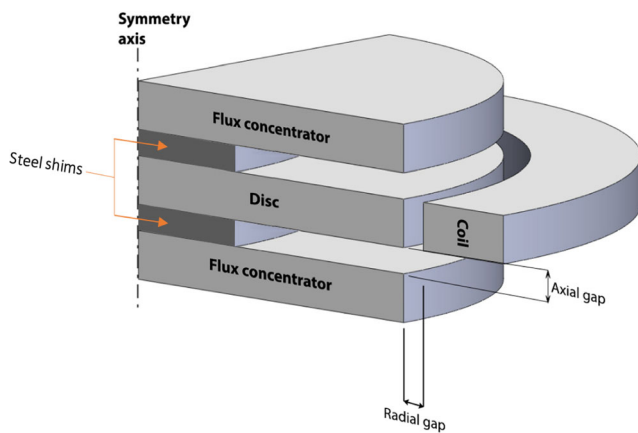Fig. 2 Axial cross-section of an induction hardened sample [20]

Fig. 3 Schematic presentation of induction heating with magnetic flux concentrators

Since the discovery of the induction phenomenon in 1831, plenty of efforts have been hailed on detecting all effective elements and improving the induction machine component to make this process more productive and user-friendly. In the last few decades, the development of computer technology has brought a great deal of facilitation in this field alongside experimental investigation. Indeed, numerical computer simulation currently plays a fundamental role in the development of this complex and multi-physical process. Investigations on residual stress profiles produced by induction surface heating and quenching [18] and numerical simulation to find a relation between induction process parameters and phase transition in surface hardening [19] can be cited as examples.

Furthermore, looking at academic researchers on induction heating and heat-treating shows applying computer modeling along with experimental has replaced the word "usefulness" with the word "necessity." Studies such as the formation of surface stresses in forming rolls hardened by induction hardening are analyzed by FEM simulation [21]. In another research, case hardening of gray and ductile iron was studied by induction hardening [22]. In a practical approach, the kinetics of structural transformation of roll steels was examined [23]. Dutka et al. [24] utilized computers along with experiments to predict phase transformation during the induction process applied for cutting tools. Also, the functionality of spray cooling was tested for induction hardening of the gearwheels [25]. Multiphysics modeling was executed to make experiments faster and more accurate for induction hardening of the ring gear [26]. Furthermore, initial microstructure and heating rate were investigated for induction hardening of 5150 steel [27]. In more recent studies, induction heating was performed to enhance the fatigue strength of AISI E52100 bearing steel [28]. Experiment analyses are also applied to study distortion of cold-drawn and induction-hardened components [29]. Jeong et al. [30] tried to predict the deformation of curve shape steel plates in high-frequency induction heating. The eddy-current method is used to define the case-depth of cast

iron hardened by induction [31]. Estimation of stress and distortion during the induction case hardening tube was performed by Nemkov et al. [32], and another experimental approach has been done to investigate the numerical modeling of the induction process [33]. To improve fatigue strength and avoid cracks in stress and strain during induction hardening, numerical simulations were performed by Ivanov et al. [34]. The effects of initial microstructure of 4140 steel on the fatigue behavior after induction hardening were also explored [35], and multiple investigations applied finite element analysis (FEA) to determine effective process parameters and to find ways for microstructural enhancement of the final induction-hardened product [36–38]. Utilizing ELTA software induction heat treatment of steel is simulated [39] wherein a combination of numerical and experimental investigations is applied for local induction hardening of large-diameter gear rolling [40]. This research team has recently utilized both experimental and FEA simultaneously to enhance induction hardening process applied to gears. 2D simulation is used to observe the effect of changing in the geometry of the component on hardness profile [41], and 3D simulation is applied to improve the case-depth of induction-hardened helical gears [42]. In another research using 2D models, the effects of induction heating process parameters on hardness profiles of 4340 steel bearing shoulders were studied [43]. The effect of frequency on the hardness profile of spline shaft heat-treated by induction is also examined [6]. Another study was focused on the effects of induction machine parameters on the case-depths of 4340 spur gear with a 2D model [44], and explore how machine parameters and geometrical factors are effective on the hardness profile of 4340 steel disc hardened by induction hardening [45]. Furthermore, surface methodology and artificial neural network modeling were exploited to observe the effects of flux concentrators on changing of edge effect in spur gear treated by induction [46]. Barglik et al. [47] recently performed a numerical study on dual frequency hardening process of a AISI 300M gear. They introduce a mathematical model of the process by the help of CCT and TTA diagrams. In 2019, Baldan et al. [48] investigated the induction heating process from another point of view, implementing multifidelity optimization approach to reduce process time. In early 2019, Li et al. [49] tried to optimize the induction heating temperature of a 55CrMo steel ball screw specimen and used the martensite fraction value as a main criterion of their study. The outcome of the study shows that the temperature increase is in favor of martensite formation and hardness gain.

This study aims at determining the most effective process parameter on edge effect in induction hardening of disc-shaped parts while flux concentrators are applied. As previously mentioned, employing disc-shaped parts in this study could helpfully eliminate some difficulties of using parts with complex geometry like gears while the result can be applied for both shapes. In this experimental effort, the ANOVA

statistical method is used to model and analyze case-depth for different combinations of process parameters and location of concentrators. This method has proved its reliability in statistic approaches and shows the way to understanding the effect and measure of each multi-physical parameter and helps to reduce errors and wasting time on calculations. In this regard, the first step is to identify the most effective range of the process parameters by preliminary tests. The second step is to plan the most effective tests with the minimum number of trials employing Taguchi planning method. The last steps are respectively performing the planned tests, statistical analysis, and then discussing the results and finally, elaborating conclusion according to the evidence. These proceeds led to yield an effective, accurate, and robust statistical model that can be used to predict the case-depth of disc-shaped workpieces. This article is formed as follows: Section 2 presents the methodology of our experimental tests based on induction surface heating and its related parameters, while results of experimentation, statistical, and sensitivity analyses are reported in Section 3. In the end, Section 4 presents conclusions and ideas for future works in this field.

2 Experimental procedure

2.1 Materials and method

Induction hardening is applied to 4340 steel discs aiming at fast surface heat treatment, which is low alloy steel known for its high toughness and strength in the heat-treated condition while preserving fatigue resistance. Mentioned characteristics make it a reliable choice for making industrial disc-shaped parts. The chemical composition of AISI 4340 steel and its mechanical characteristics are noted in Tables 1 and 2 respectively.

The induction heating machine that is used for this study employs two generator sets of a medium and high frequency to produce a wide range of frequencies. The maximum range of frequency, approximately 1 MW, could be achieved by a combination of the two generators. Here is the machine procedure to drive the maximum range of frequency: first is to create maximum power of 550 kW by using audio-frequency technology with solid-state converters that operate at 10 kHz, and the second is to deliver maximum power of 450 kW by running a transistor radiofrequency generator at 200 kHz. To achieve high frequency, a thyristor radiofrequency (RF)

generator operates at 200 kHz. Process controlled utilizing real-time monitoring (RTM) module to ensure the state of machine parameters during the process validating whether the actual parameters are the same as the input parameters.

A disc is positioned on a ready-made stand kit between two magnetic flux concentrators. Discs and flux concentrators are in the same material, shape, and geometry; AISI 4340 steel with an outer diameter of 104.3 mm, and a thickness of 6.5 mm. AISI 1010 steel shims are inserted between disc and concentrators to ensure distance between them (axial gap). The thickness and the outer diameter of each shim are 0.2 ± 0.05 mm and 31.75 mm respectively. The geometrical specification of copper-made coil is 140 mm for the outer diameter and 110 mm for the inner diameter with a useful section of 7 mm × 7 mm and thickness of 2 mm. Figure 3 displays a schematic position of magnetic flux concentrators, master disc, and coil. Finally, a jet of a cooling solution containing 92% water and 8% of polymers is used as coolant fluid for quenching the disc after induction heating. It should be mentioned that all disc samples have undergone a uniform quenching and tempering treatment to have approximately a uniform hardening of 45 HRC through the discs. This is to prepare an equal initial condition for all samples before starting the induction heating process. As previously mentioned, because of the variety of flux densities in different areas of the disc, different amounts of heat will be generated through the disc and can be stocked in some areas. Therefore, the area that is exposed to the more magnetic flux is considered critical that must be heated within the range of austenization (above Ac_3) to avoid overheating more or less than this specific temperature range. To serve this purpose, a typical guideline for the induction hardening of the AISA 4340 disc is followed.

To avoid useless trial and error tests, an optimized number of tests should be done; therefore, a rigid method for designing the experiments is adopted to provide the maximum amount of information from the minimum number of experiments. In this study, the Taguchi planning method is applied because of the capability of this method in executing efficient and simplified factorial results [52, 53]. To apply this optimized experimental planning method, a list of effective parameters is required with a defined level of each. During the induction heating, machine power, heating time, and frequency are three input variables of the induction machine that control the generated heat and consequently the temperature amplitude on the part. It should be considered, in contrast to the power and

Table 1 AISI 4340 steel chemical composition in wt% [50]

Element	Ni	Cr	Mn	C	Mo	Si	S	P
Content (%)	1.65–2.00	0.70–0.90	0.60–0.80	0.38–0.43	0.20–0.30	0.15–0.30	0.04	0.035

Table 2 Mechanical properties of AISI 4340 steel [51]

Yield strength (MPa)	Ultimate tensile strength (MPa)	Elongation at break (%)	Hardness Rockwell C (HRC)
710	1110	13.2	35

heating time, frequency is not tunable. Other effective factors are the axial gap (the gap between each concentrator and master disc), and the radial gap (the gap between the coil and discs) as shown in Fig. 3. Accordingly, the input parameters are power, time, axial, and radial gap. The levels of input parameters and their ranges were defined by low, medium, and high levels as presented in Table 3. Regarding the abbreviation list in Table 3, in the following, P, T, AG, and RG are used instead of power, heating time, axial gap, and radial gap respectively.

Taguchi experiment planning is well-known as one of the most reliable and robust planning-designers to perform a minimum efficient number of experiments. A proper range of factors by preliminary tests along with using Taguchi experimental design makes the process more robust, efficient, and with a minimum number of trials [54, 55]. Indeed, performing an induction hardening within the maximum and minimum range of parameters is of critical importance to create maximal and minimal case-depth transformation. An L_9 orthogonal matrix corresponding to nine (9) experimental tests is addressed by the Taguchi planning method; consequently, each test consisted of a unique combination of parameter levels as shown in Table 4.

2.2 Micro-indentation hardness tests

Micro-indentation tests using Clemex machine are performed to measure the hardness of specimens at their cross-section. After surface-hardening process by induction heating method, discs specimens are cut into two halves. In the following, the middle plane refers to the surface that cut the thickness of disc in two equal parts parallel to the edge plane. The edge plane, in its turn, refers to the outer surfaces of the disc as depicted in Fig. 4. Micro-indentation tests are then performed in both edge and middle planes, and results are summarized in Table 5. These responses present the measured case-depths

of discs at the edge and middle of discs respectively denoted as d_E, d_M. It worth mentioning that the defined case-depths on edge planes are calculated as the mean value of case-depths measured on the two exterior surfaces of the disc (edge planes). Doing so could avoid complications in analyses related to outliers.

The results in Table 5 imply that the maximum case-depth in both middle and edge planes occurred using test 9 parameters, while the minimum case-depth in middle and edge planes is observed in test 1. In detail, results of tests 9 and 1 are presented in Fig. 5a and b, in which the hardness profile of induction heat-treated discs is evaluated. Three distinguished regions could be defined in these figures; the first region presents a hardened surface layer due to martensitic phase formation (the line approximately parallel horizontal axis), the second region displays a hardness drop to approximately the core material hardness (the part with deep slope), and the third region in which discs tempered before the tests and preserve the initial core material hardness (approximately 45 HRC) [56]. Figure 5a demonstrates the hardness profile and obtained case-depth at edge plane (d_E) resulted respectively from test 9 and test 1, while Fig. 5b shows the hardness profile and case-depth at the middle plane (d_M).

There are three main conclusions to be drawn from Table 4. First, the maximum case-depth at the edge plane happens in the maximum level of power and axial gap, and a minimum level of radial gap. Meanwhile, the minimum case-depth at edge plane occurs when P, T, AG, and RG are set at their minimum level. Second, the minimum amplitude of the case-depth difference between middle and edge planes (Δd), which is an indication of reaching a minimum edge effect, is

Table 3 Experimental factors and range of values for each level

Parameter	Unit	Abbreviation	Level 1	Level 2	Level 3
Power	kW	P	85.0	100.0	115.0
Time	s	T	0.40	0.50	0.60
Axial gap	mm	AG	0.20	0.80	1.40
Radial gap	mm	RG	2.60	2.80	3.10

Table 4 Design of experiences, L_9 orthogonal matrix

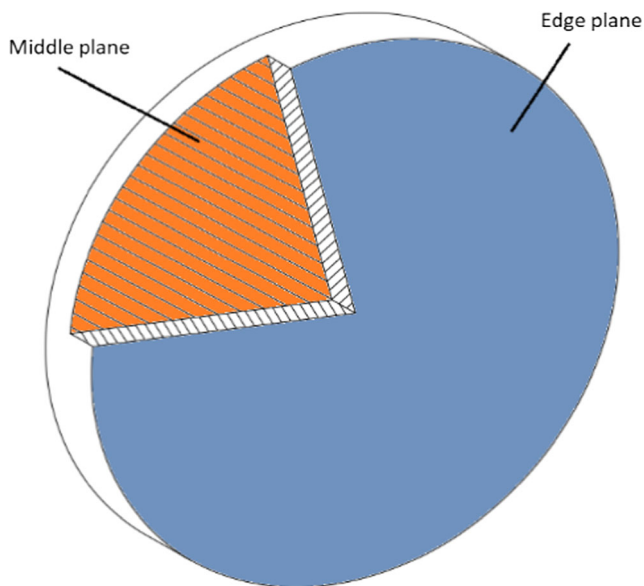| Test no.	AG (mm)	P (kW)	T (s)	RG (mm)
1	0.2	85	0.4	2.6
2	0.2	100	0.5	2.8
3	0.2	115	0.6	3.1
4	0.8	85	0.5	3.1
5	0.8	100	0.6	2.6
6	0.8	115	0.4	2.8
7	1.4	85	0.6	2.8
8	1.4	100	0.4	3.1
9	1.4	115	0.5	2.6

Fig. 4 Schematic of the disc representative for middle and edge planes

reached when heating time is in its maximum level of variations. Third, a proper variation of process parameters in terms of covering the measured maximum and minimum case-depths confirms the credibility of designed tests based on Taguchi method.

3 Effects of parameters on hardness profile

3.1 Statistical analysis and parameters contribution

To estimate the effectiveness degree of each variable in the experimental, outputs are analyzed utilizing the statistical method of analysis of variance (ANOVA) [57, 58]. ANOVA uses an F-test to appraise the regression model. To evaluate the degree of parameters' participation in responses (case-

Table 5 Microhardness test results in middle plane (d_M) and edge plane (d_E)

Test no.	Parameters (variables)				Responses	
	AG (mm)	T (s)	P (kW)	RG (mm)	d_E (mm)	d_M (mm)
1	0.2	0.4	85	2.6	0.525	0.90
2	0.2	0.5	100	2.8	1.225	1.30
3	0.2	0.6	115	3.1	1.475	1.550
4	0.8	0.5	85	3.1	0.80	1.050
5	0.8	0.6	100	2.6	1.575	1.550
6	0.8	0.4	115	2.8	1.125	1.250
7	1.4	0.6	85	2.8	1.30	1.30
8	1.4	0.4	100	3.1	0.930	1.10
9	1.4	0.5	115	2.6	1.725	1.550

depth at middle and edge planes), the main effect diagram for each dependent variable (specific range combination of the parameters) is first plotted. The results of ANOVA concerning the case-depth at edge and middle planes are shown in Tables 6 and 7 respectively. In these tables, the degrees of freedom (DoF), sum of squares, contribution percentage, F-value, and p-value are the terms that declare the results of the analyses. Also, to estimate the precision of the regression model, the coefficient of determination (denoted by R^2 or R-squared) is calculated. The term p-value determines statistically whether the effect of process parameters on the case-depth is significant. In other words, ANOVA calculates the p-value and compares it with the significance level (α) to determine whether the null hypothesis is rejected. In fact, the null hypothesis states that the effect of studied parameters is insignificant. The null hypothesis can be rejected when the calculated p-value is lower than or equal to the designated significance level. The defined significance level (α) for this study is 95%, which means that there is a 5% risk of considering a specific parameter as having a noticeable effect on the process when there is no real effect.

Linear regression is then performed based on ANOVA results to develop predictive equations for case-depths in the edge and middle planes (d_E and d_M respectively) as a function of power (P), heating time (T), axial gap (AG), and radial gap (RG). Here outputs are case-depths that are termed dependent variable, and input parameters of P, T, AG, and RG are termed independent variables. The ANOVA conditions in this study are selected as a stepwise method wherein interactions between factors are included. The stepwise method aims at excluding less important factors and interactions in each step giving more importance to the effective factors. Analyses were proceeded by including the most important interactions to prevent changing the meaning of the lower order coefficients. Furthermore, involving any redundant term to the model while the related P-value is higher than 0.05 could make the model more complicated [59].

P-values for T, P, P×AG, and RG are respectively 0.001, 0.002, 0.030, and 0.060 as given in Table 6. Except for RG, all p-values are less than 0.05; hence, the null hypothesis is rejected. It can be observed that in d_E, the heating time (T) and machine power (P) are the most effective parameters on the case-depth and then, P×AG with less degree of importance regarding their descending quantity of p-values. P-value of 0.030 for P×AG connotes interaction between power and the axial gap was in such a way that combining these two independent variables gave a different effect on d_E. Table 7 introduces P, T, T×RG, and RG as the most effective variables in d_M concerning the P-values (respectively 0.00, 0.005, 0.015, and 0.031). Results for both d_E and d_M prove the involving interactions as the P-values of P×AG and T×RG are respectively 0.030 and 0.015 from Tables 6 and 7. The contribution of each variable and interaction is also defined in the edge and
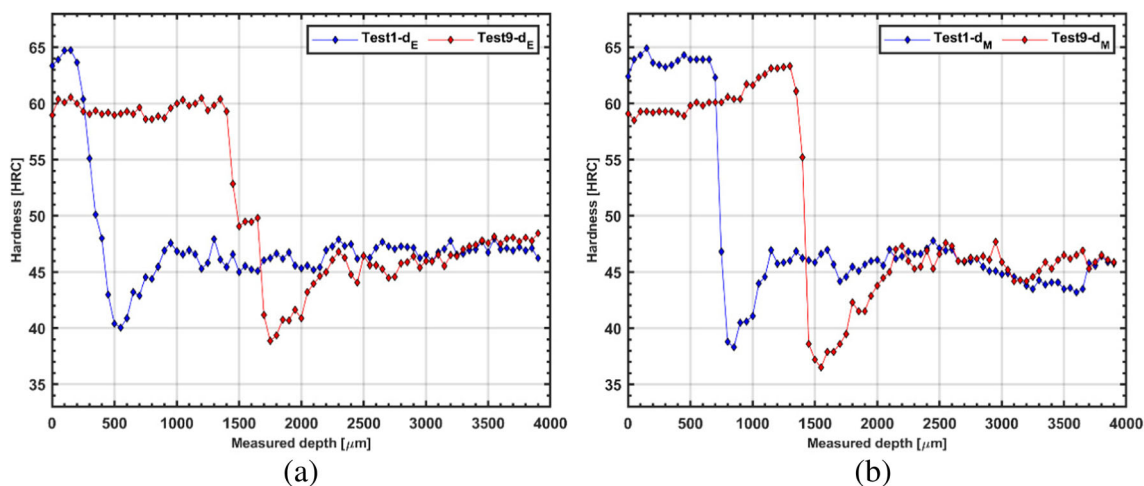
Fig. 5 Hardness profile of test 1 and test 9; **a** in middle plane d_E, **b** in edge plane d_M

middle planes of the disc. From ANOVA results in Table 6, it can be concluded that in d_E, P and T have the main effect on the response as their contribution is respectively 40.31% and 43.69%. In d_M, the contribution of P and T indicates their dominant effect in the response is slightly more than their effect in d_E as their ratios are respectively 44.81% and 48.98%.

3.2 Main effect plot and predictive regression models

To define the correlation between each independent variable and dependent variable, main effect plots are drawn. Interpretation by plots provides us a visual trend of response variation with respect to parameter levels. This approach allows exploiting a goodness-of-fit model that describes the relationship between variables and predicting the case-depth with a combination of the input parameters. Main effect plots are drawn in Matlab^{TM} to describe the most effective parameters affecting the response. These plots show a general trend of how one parameter affects the response allowing their effectiveness comparison separately. This is performed by verifying the slope of each variation line between two levels in which the steeper the slope, the more effective the parameter on the response. The main effect plots of the responses (d_E and

d_R) over the 3 levels of their parameters (P, T, RG, and AG) are shown in Fig. 6. In this figure, d_E and d_R are presented with respectively blue and red lines. It can be observed from Fig. 6 for d_E that P and T have a significant effect on the case-depth. The bigger domain of changing in response with steeper variation lines is the evidence of this interpretation. The effect of the axial and radial gap (AG and RG) on the case-depth at edge plane is less compared to P and T. This observation is based on the fact that the slope of AG and RG variation is less than the one of P and T. Like d_E, P and T are the effective parameters on d_M wherein the slopes of variations are steep. The effect of AG and RG on d_M can be interpreted as less than P and T since their variation slop is much smaller. Compared to AG, increasing in RG shows the opposite effect on the response as it is vivid from the negative slop from levels 1 to 3.

The main effect plots are used to reveal the relationship of each independent variable on the dependent variables. The interaction between the parameters is also studied based on ANOVA as a combination of interacting variables because the effect of one variable depends on the value of the other [55]. Studying the interaction of variables indicates that P and AG (P×AG) in edge plane (d_E) and T and RG (T×RG) in middle

**Table 6** Results of ANOVA for micro-hardness tests in edge plane (d_E)

Factors	DoF	Sum of squares	Contribution	F-value	P-value
P	1	0.48167	40.31%	46.21	0.002
T	1	0.52215	43.69%	66.03	0.001
RG	1	0.06695	5.60%	6.73	0.060
P*AG	1	0.09084	7.60%	10.86	0.030
Error	4	0.03345	2.80%		
Total	8	1.19505	100.00%		

Table 7 Results of ANOVA for micro-hardness tests in the middle plane (d_M)

Factors	DoF	Sum of squares	Contribution	F-value	P-value
P	1	0.201667	44.81%	331.70	0.000
T	1	0.220417	48.98%	29.76	0.005
RG	1	0.014803	3.29%	10.76	0.031
T*RG	1	0.010607	2.36%	16.92	0.015
Error	4	0.002507	0.56%		
Total	8	0.450000	100.00%		

Fig. 6 Main effect plots of case-depth on middle and edge planes (d_M and d_E)
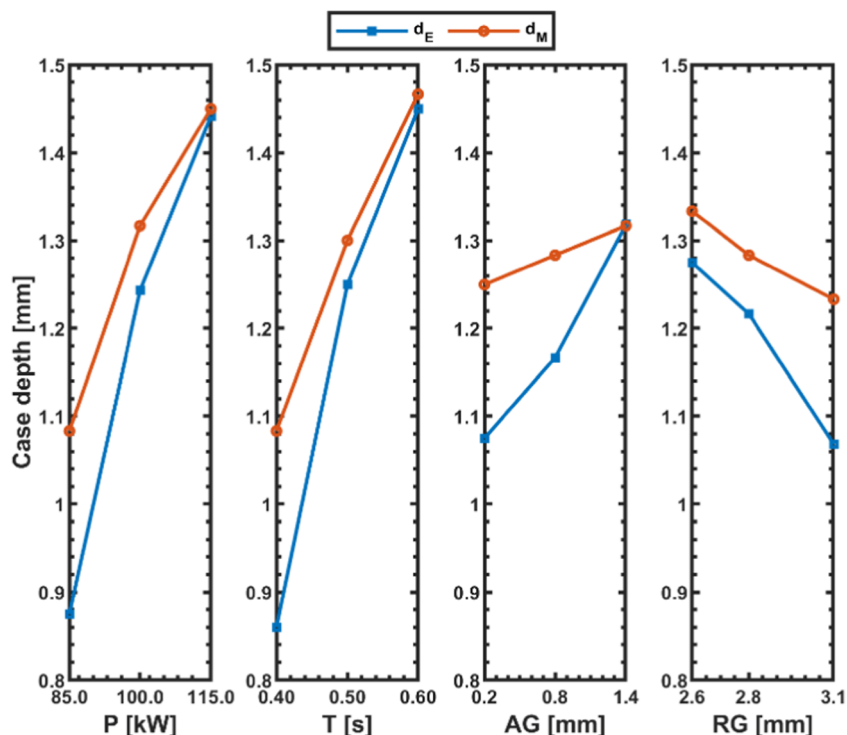
plane (d_M) present interactions. To this end, a predictive linear regression of case-depth, which is a function of the important input parameters and interactions, is exerted for the edge and middle plane. These predictive functions are respectively presented in Eqs. (1) and (2).

$$d_E = -1.130 + 0.01725 \times P + 3.042 \times T - 0.386 \times RG$$
$$+ 0.002046 \times P \times AG \tag{1}$$

$$d_M = -3.269 + 0.012450 \times P + 7.73 \times T + 0.829$$
$$\times RG - 2.053 \times T \times RG \tag{2}$$

The coefficient of determination (R^2) concerning the regression equation of d_E is 97% which declares that the predictive equation represents 97% of the response behavior based on the presented factors and their interactions. The R^2 of d_M is calculated 99% which means that the predictive regression equation represents almost perfectly the variation of response (d_M) in the range of experimentations. The accuracy of regression equations can also be estimated based on the residual evaluations. In this regard, the difference between predicted and measured values represents the possible regression error (residual). Using Eq. (3), the relative error of predicted models can be calculated. Our study's outcomes indicate a good agreement between experimentally measured and predicted model for case-depths at the edge plane (d_E) and the middle plane (d_M). The estimated errors of d_E are less than 4% except for test 2 where it reaches approximately 12% while the error of d_M is less than 4% for all tests.

$$Error\ (\%) = \frac{\left|\ Predicted - Measured\ \right|}{Measured} \times 100 \tag{3}$$

The goodness of fit, which visually represents the level of agreement between the measured experiments and predicted models, is depicted in Fig. 7a and b for d_E and d_M case-depths respectively. Predicted values that agree exactly with measured values would fall on the red line, while the dispersion of these values (blue points) with respect to the red line represents the lack of fitness. The plots of Fig. 7 illustrate a very good agreement between the experimental values and predictive models, for which the predicted model of d_M fits better than d_E.

3.3 Response surfaces and sensitivity analysis

For empirical modeling, response surface methodology (RSM) is applied whereby the results are shown by contour plots. Contour plots are 3D diagrams that the response curve is projected on the plane of variables. In this regard, the response is shown by contours (color gradient and isolines) on the plane of variables. Here the variables are P, T, AG, and RG, and responses are d_E and d_M. The results of RSM are displayed in Fig. 8 for d_E and in Fig. 9 for d_M. It should be noted that the non-presented parameters in the plots are considered as a constant independent variable in their medium level of 100 kW, 0.5 s, 0.8 mm, and 2.8 mm for P, T, AG, and RG respectively.
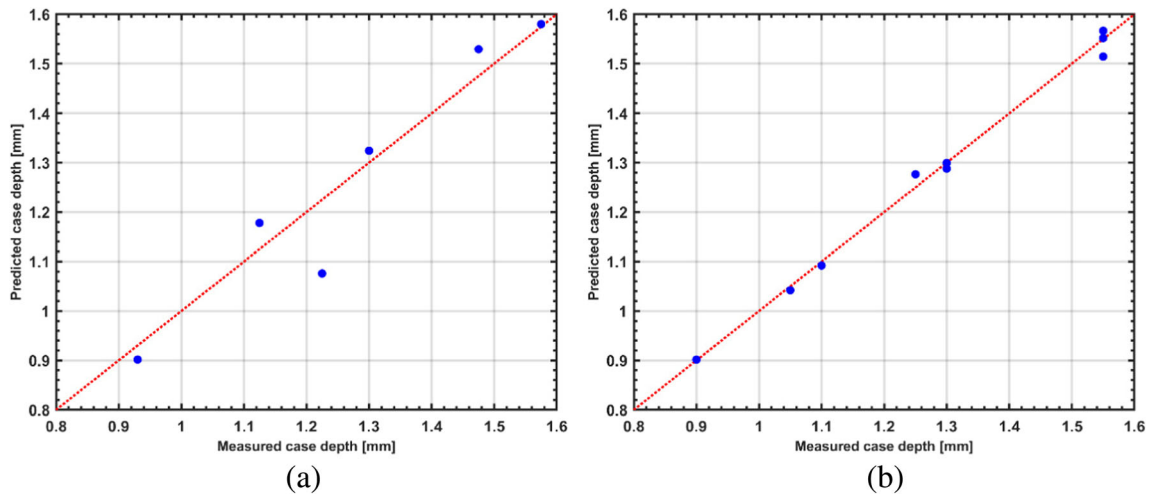
(a)　　　　　　　　　　　　　　　　　　　　(b)

Fig. 7 Case-depth measured by experiments versus predicted by regression equations in **a** edge plane (d_E) and **b** middle plane (d_M)

A contour plot of case-depths in edge plane (d_E) versus P and T is illustrated in Fig. 8a wherein the maximum values of case-depth (1.7 mm) in the upper right corner of the plot correspond to the highest values of both P and T. The minimum value of case-depth (0.7 mm) in this graph corresponds

with the lowest values of both P and T. In other words, both T and P have an increasing effect on the case-depth value as well as approximately the same impact on the cade depth enhancement. The same trend can be observed in Fig. 8b and c for P and AG as well as T and AG, but the case-depth value is
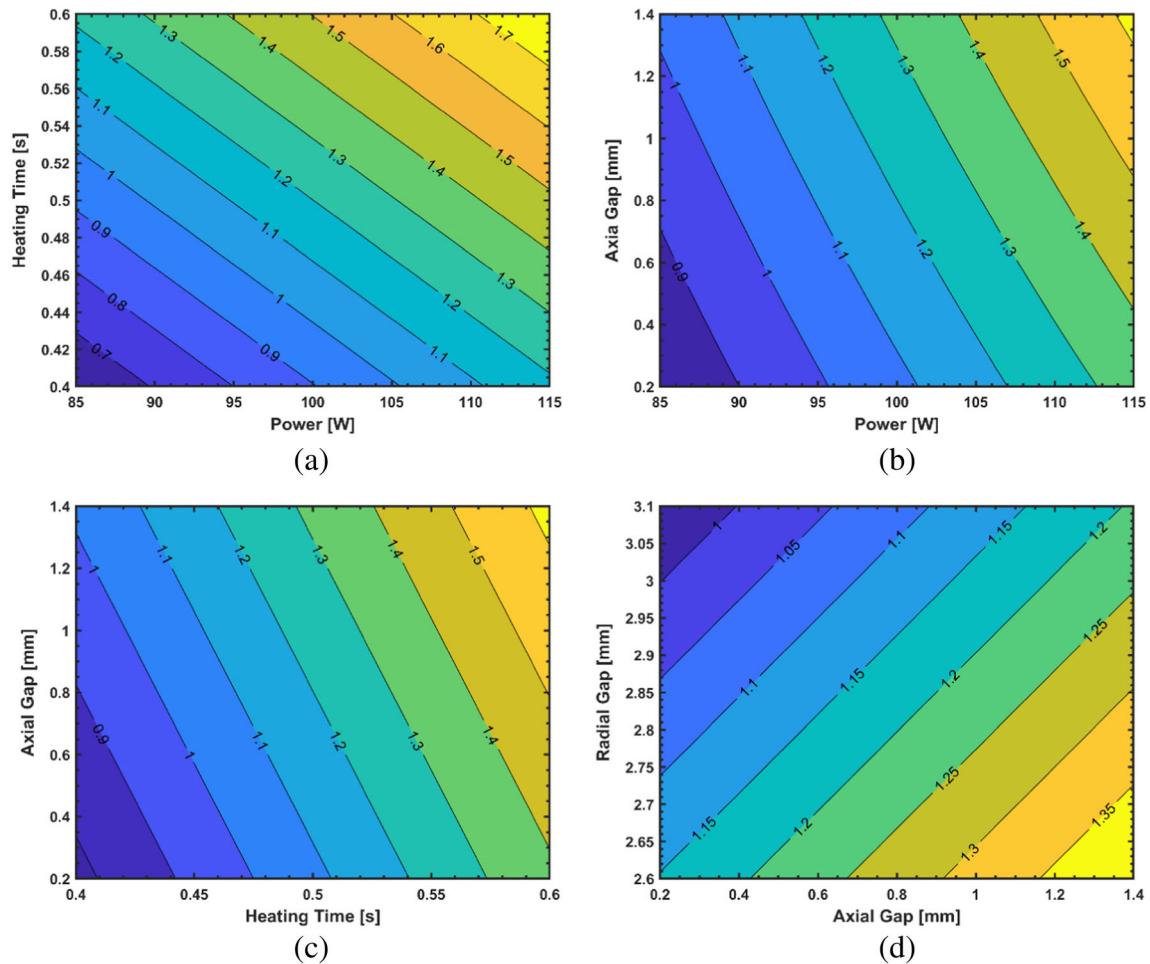

(a)　　　　　　　　　　　　　　　　　　　　(b)

(c)　　　　　　　　　　　　　　　　　　　　(d)

Fig. 8 Contour plots of Power (P), Heating Time (T), Axial Gap (AG), and Radial Gap (RG) versus case-depths at edge plane of discs (d_E)
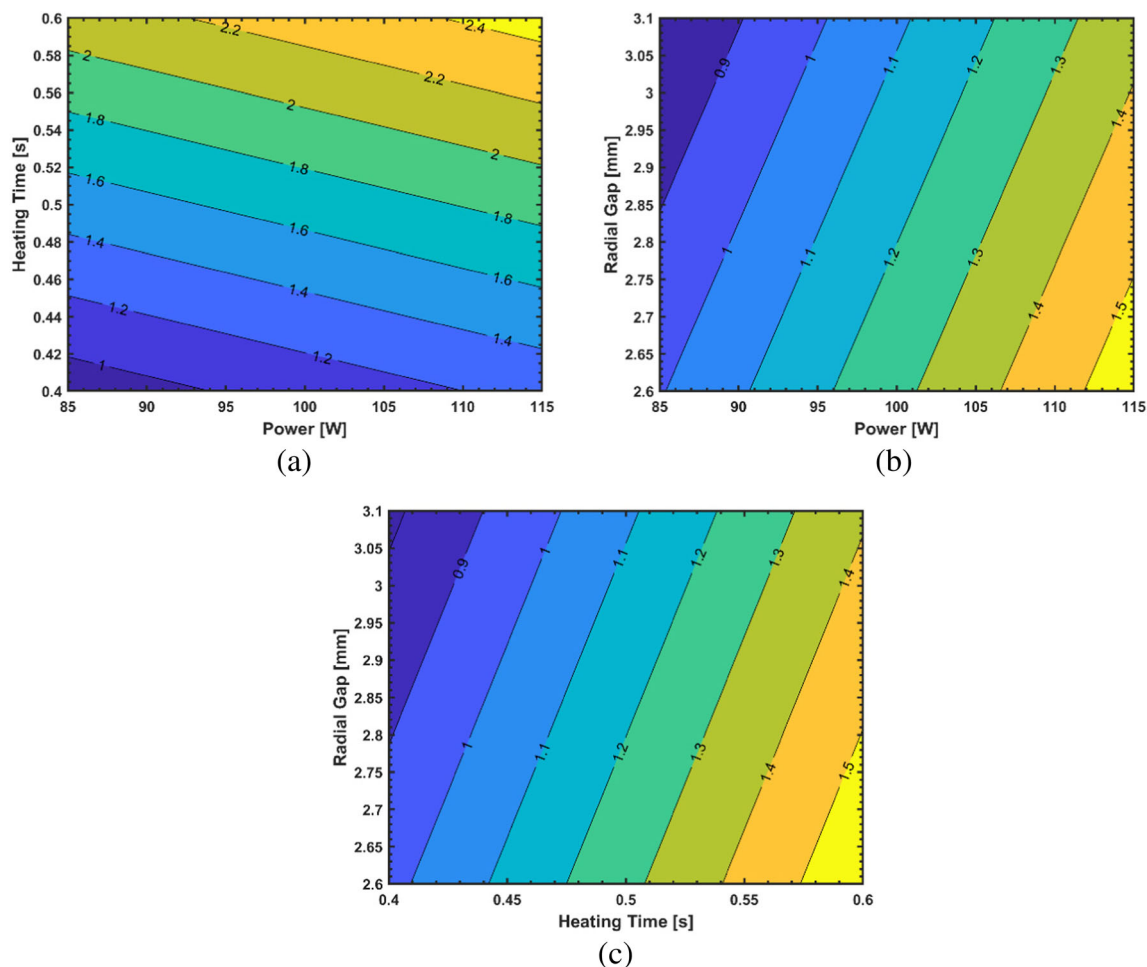
Fig. 9 Contour plots of Power (P), Heating Time (T), and Radial Gap (RG) versus case-depths at middle plane of discs (d_M)

affected more by changes in P and T than AG in these plots. As it is already explained in Section 3.2 and can be observed in Fig. 8d, RG shows the opposite effect on the case-depth when it is compared with other parameters and the maximum case-depth happens at minimum RG. This is demonstrated in the contour plot of case-depths at edge plane versus AG and RG. As a conclusion, the highest case-depth can be achieved by increasing P, T, and AG whereas decreasing RG.

Based on ANOVA in Section 3.1, the most effective parameters of case-depths in middle plane (d_M) are defined as P, T, and RG in which their contour plots are presented in Fig. 9. The increase of P and T results in the case-depth increase as shown in Fig. 9a. Similar to d_E, RG has an inverse effect on d_M as illustrated in Fig. 9b and c. It can be concluded from Fig. 9 that case-depth in middle plane of discs is mainly affected by the P and T in which their increase would increase the case-depth.

4 Edge effect discussion

Considering the principle of magnetic fields, they are denser near the source of the field. Consequently, moving from the outer diameter of the disc toward the center of the disc hardness profile is reduced considerably to around the initial hardness of material as is shown in Fig. 5. Loops of induced electrical currents, namely "eddy currents" arising from changes in the magnetic field, tend to be stuck in corners that lead to non-uniform thermal distribution through the disc. Therefore, a non-uniform hardness profile and finally a different case-depth profile in edge plane versus the middle plane are formed. To make a comparison of case-depth profiles in the edge and middle planes, in this section, the middle plane is considered as the reference plane and the differences between the planes ($\Delta d = d_E - d_M$) present the edge effect. The ultimate purpose of this study is to determine the best combination of process parameters that maximized the case-depth with minimum edge effect utilizing flux concentrators. To this end, the less the Δd, the less the edge effect that results in a more desirable uniform case hardening.

The effects of induction hardening process parameters (P, T, RG, and AG) on the case-depth profile have been already discussed separately in the middle and edge planes. Results showed that the case-depth profile is mainly affected by P and T, while other parameters including RG and AG participated

less. In this study, the interaction of parameters is also considered and regarding ANOVA, only P×AG and T×RG are effective parameters in case-depth. Applying the concept of Δd, and presenting it in Fig. 10, a reducing trend in edge effect from test 1 to test 9 can be observed. The minimum edge effect is then noted in test 7 and test 5. The experiment parameters, P, T, AG, and RG for test 7, are 85 kW, 0.6 s, 1.4 mm, and 2.8 mm respectively which refers to the low-level of machine power, the maximum level of T and AG, and mid-level of RG. The process parameters of test 5 are 100 kW, 0.6 s, 0.8 mm, and 2.6 mm, respectively, for P, T, AG, and RG. They refer to the maximum level of P and T as well as the mid-level of AG and RG. It is worth mentioning that the average case-depth in test 7 is 1.30 mm while in test 5 is 1.56 mm. Although the best case-depth results in test 9, the edge effect is also considerable. It could be concluded that the best scenario, deeper case-depth, and less edge effect occurred in tests 5 and 7 where the heating time is tuned in its maximum level, the machine power, and radial gap are in low and mid-levels, and the axial gap in its maximum and mid-levels.

5 Conclusions

4340 steel discs are used in this study to investigate the effects of induction hardening process parameters on the case-depth and edge effect with the presence of magnetic concentrators. The process parameters, machine power (P), heating time (T), the axial gap between disc and concentrator (AG), and the radial gap between disc and coil (RG) are considered to evaluate two responses, case-depth in edge and middle of discs (d_E and d_M). The Taguchi design method is employed to plan nine tests (L_9) in three-parameter variation levels. The micro-hardness test and
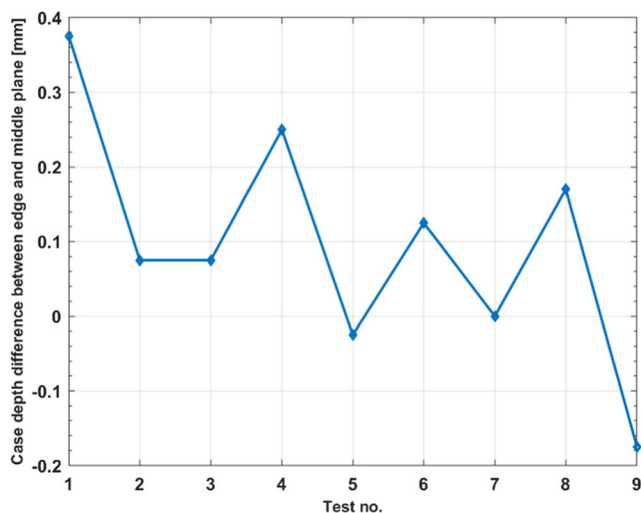
consequently the case-depths are then analyzed by analysis of variance (ANOVA). Using linear regression, predictive models are then developed for d_E and d_M with the coefficient of determination (R^2) of 97% and 99% respectively. The analyses show that heating time and machine power are dominant parameters to control the case-depth in d_E and d_M as far as the contribution percentages of T and P for d_E are respectively 43.69% and 40.31%. Taking into account the effect of parameter interactions, P×AG is contributed 7.60%. In d_E variation, the contribution of T, P, RG, and T×RG in the variation of d_E is 48.98%, 44.81%, 3.29%, and 2.36%. Moreover, contour plots based on response surface methodology (RSM) show that setting independent variables of P, T, and AG at maximum level and RG at minimum level would enhance the case-depths (d_E and d_M). The edge effect, which presents the non-uniformity of case-depth in the edge plane with respect to the middle plane, is then analyzed in which tests 5 and 7 present the minimum edge effect. Based on the test results, maximum heating time, medium machine power, and radial gap as well as maximum axial gap help reduce the edge effect. It is worth mentioning that the average case-depth in tests 5 and 7 reaches 1.56 and 1.30 mm respectively. The results of this study can also be used in disc-shaped parts such as gears.

Although the results of this study are promising, some improvements and applications can be foreseen. Future works can study the generator frequency fluctuation according to the variation of geometrical factors (thickness, axial, and radial gaps) as an induction machine factor. Moreover, the concentration thickness can be optimized during the extensive design of experiments. To optimize surface treatment of the other parts like bevel gears, and helical gears which have different and more complex shapes, experimental test benches as well as predictive models can be developed. In this regard, applying artificial intelligence to create and enhance the models could be the next project to perform.

Fig. 10 Case-depth difference between middle plane and edge plane (Δd) resulted from the 9 arrays of experiments

Declarations

Ethical approval   This article does not involve human or animal participation or data; therefore, ethics approval is not applicable.

Consent to participate   This article does not involve human or animal participation or data; therefore, consent to participate is not applicable.

Consent to publish   This article does not involve human or animal participation or data; therefore, consent to publication is not applicable.

Competing interests   The authors declare no competing interests.

References

1. Gao K, Qin X, Wang Z, Chen H, Zhu S, Liu Y, Song Y (2014) Numerical and experimental analysis of 3D spot induction hardening of AISI 1045 steel. Journal of Materials Processing Technology 214(11):2425–2433

2. Shokouhmand H, Ghaffari S (2012) Thermal analysis of moving induction heating of a hollow cylinder with subsequent spray cooling: effect of velocity, initial position of coil, and geometry. Applied Mathematical Modelling 36(9):4304–4323

3. Semiatin SL, Stutz DE (1985) Induction heat treatment of steel

4. Rudnev V, Loveless D, Cook RL (2017) Handbook of induction heating. CRC press

5. Tong D, Gu J, Totten GE (2018) Numerical investigation of asynchronous dual-frequency induction hardening of spur gear. International Journal of Mechanical Sciences 142:1–9

6. Hammi H, El Ouafi A, Barka N (2016) Study of frequency effects on hardness profile of spline shaft heat-treated by induction. Journal of Materials Science and Chemical Engineering 4(03):1

7. Rudnev V (2008) Induction hardening of gears and critical components. Gear Technol 58–63

8. Mahyar Parvinzadeh SSK, Omidi N, Barka N, Khalifa M (2021) A novel investigation into edge effect reduction of 4340 steel spur gear during induction hardening process. Int J Adv Manuf Technol 1–15. https://doi.org/10.1007/s00170-021-06639-w

9. Iron GC (1998) Metals Handbook Desk Edition. In: Davis JR (editor) p 309–314

10. Fisk M, Lindgren L-E, Datchary W, Deshmukh V (2018) Modelling of induction hardening in low alloy steels. Finite elements in analysis and design 144:61–75

11. Rajan T, Sharma C, Sharma A (2011) Heat treatment: principles and techniques. PHI Learning Pvt. Ltd.

12. Putatunda SK (2003) Influence of austempering temperature on microstructure and fracture toughness of a high-carbon, high-silicon and high-manganese cast steel. Materials & design 24(6): 435–443

13. Callister WD, Morin A (2001) Science et génie des matériaux. Dunod

14. Doyon G, Rudnev V, Russell C, Maher J (2017) Revolution-not evolution-necessary to advance induction heat treating. Advanced Materials & Processes 175(6):72–80

15. Savaria V, Bridier F, Bocher P (2016) Predicting the effects of material properties gradient and residual stresses on the bending fatigue strength of induction hardened aeronautical gears. International Journal of Fatigue 85:70–84

16. Barka N, Bocher P, Brousseau J (2013) Sensitivity study of hardness profile of 4340 specimen heated by induction process using axisymmetric modeling. The International Journal of Advanced Manufacturing Technology 69(9-12):2747–2756

17. Rao S, McPherson D (2003) Experimental characterization of bending fatigue strength in gear teeth. Gear Technology 20(1):25–32

18. Grum J (2007) Influence of induction surface heating and quenching on residual stress profiles, followed by grinding. International Journal of Materials and Product Technology 29(1-4):211–227

19. Kurek K, Dolega DM (2007) Numerical simulation of superficial induction hardening process. International Journal of Materials and Product Technology 29(1-4):84–102

20. Khalifa M (2019) Étude du profil de dureté et de l'effet de bord des disques et engrenages droits traités thermiquement par induction en utilisant les concentrateurs de flux: prédiction et optimisation numérique et expérimentale. Université du Québec à Rimouski

21. Pokrovskii A, Leshkovtsev V, Polushin A, Bochektueva E (2011) Simulation of structural state and stresses in forming rolls subjected to hardening with induction heating. Metal Science and Heat Treatment 52(9-10):442–445

22. Balachandran G, Vadiraj A, Sharath B, Krishnamurthy B (2010) Studies on induction hardening of gray iron and ductile iron. Transactions of the Indian Institute of Metals 63(4):707–713

23. Polushin A, Kamantsev S, Gryzunov V, Minakov MY (2010) Kinetics of hardened layer formation with induction hardening. Metal Science and Heat Treatment 52(7-8):388–392

24. Dutka V, Maistrenko A, Lukash V, Mel'nichuk O, Virovets L (2012) Computer-aided and experimental study of hardness distribution in cutting tool steel body due to phase transformations during induction hardening. Journal of Superhard Materials 34(2): 131–140

25. Rodman D et al (2011) Induction hardening of spur gearwheels made from 42CrMo4 hardening and tempering steel by employing spray cooling. steel research international 82(4):329–336

26. Candeo A, Ducassy C, Bocher P, Dughiero F (2011) Multiphysics modeling of induction hardening of ring gears for the aerospace industry. IEEE Transactions on Magnetics 47(5):918–921

27. Clarke K, Van Tyne C, Vigil C, Hackenberg R (2011) Induction hardening 5150 steel: effects of initial microstructure and heating rate. Journal of materials engineering and performance 20(2):161–168

28. Santos E, Kida K, Honda T, Koike H, Rozwadowska J (2012) Fatigue strength improvement of AISI E52100 bearing steel by induction heating and repeated quenching. Materials Science 47(5):677–682

29. Hirsch TGK, da Silva Rocha A, Nunes RM (2013) Distortion analysis in the manufacturing of cold-drawn and induction-hardened components. Metallurgical and Materials Transactions A 44(13): 5806–5816

30. Jeong C-M, Yang Y-S, Bae K-Y, Hyun C-M (2013) Prediction of deformation of steel plate with forced displacement and initial curvature in a forming process with high frequency induction heating. International Journal of Precision Engineering and Manufacturing 14(5):785–790

31. Nateq MH, Kahrobaee S, Kashefi M (2013) Use of eddy-current method for determining the thickness of induction-hardened layer in cast iron. Metal Science and Heat Treatment 55(7-8):370–374

32. Nemkov V, Goldstein R, Jackowski J, Ferguson L, Li Z (2013) Stress and distortion evolution during induction case hardening of tube. Journal of materials engineering and performance 22(7): 1826–1832

33. Schwenk M, Hoffmeister J, Schulze V (2013) Experimental determination of process parameters and material data for numerical modeling of induction hardening. Journal of materials engineering and performance 22(7):1861–1870

34. Ivanov D, Markegård L, Asperheim JI, Kristoffersen H (2013) Simulation of stress and strain for induction-hardening applications. Journal of materials engineering and performance 22(11):3258–3268

35. Hayne M, Anderson P, Findley K, Van Tyne C (2013) Effect of microstructural banding on the fatigue behavior of induction-hardened 4140 steel. Metallurgical and Materials Transactions A 44(8):3428–3433

36. Spezzapria M, Forzan M, Dughiero F (2015) Multiphysical-multiscale FEM simulation of contour induction hardening on aeronautical gears

37. Hömberg D, Liu Q, Montalvo-Urquizo J, Nadolski D, Petzold T, Schmidt A, Schulz A (2016) Simulation of multi-frequency-induction-hardening including phase transitions and mechanical effects. Finite Elements in Analysis and Design 121:86–100

38. Gao K, Wang Z, Qin X-p, Zhu S-x (2016) Numerical analysis of 3D spot continual induction hardening on curved surface of AISI 1045 steel. Journal of Central South University 23(5):1152–1162

39. Bukanin V, Zenkov A, Ivanov A, Nemkov V (2016) Simulation of induction heat treatment of steel articles with the help of ELTA 6.0 and 2DELTA software. Metal Science and Heat Treatment 58(7-8): 493–497

40. Fu X, Wang B, Zhu X, Tang X, Ji H (2017) Numerical and experimental investigations on large-diameter gear rolling with local induction heating process. The International Journal of Advanced Manufacturing Technology 91(1-4):1–11

41. Barka N, Bocher P, Brousseau J, Arkinson P (2012) Effect of dimensional variation on induction process parameters using 2D simulation, in Advanced Materials Research, vol. 409: Trans Tech Publ, pp. 395-400

42. Barka N, Chebak A, El Ouafi A (2013) Simulation of helical gear heated by induction process using 3D model, in Advanced Materials Research, vol. 658: Trans Tech Publ, pp. 266-270

43. Hammi H, Barka N, El Ouafi A (2015) Effects of induction heating process parameters on hardness profile of 4340 steel bearing shoulder using 2D axisymmetric model. International Journal of Engineering and Innovative Technology 4:41–48

44. Barka N (2017) Study of the machine parameters effects on the case-depths of 4340 spur gear heated by induction—2D model. The International Journal of Advanced Manufacturing Technology 93(1-4):1173–1181

45. Khalifa M, Barka N, Brousseau J, Bocher P (2019) Sensitivity study of hardness profile of 4340 steel disc hardened by induction according to machine parameters and geometrical factors. The International Journal of Advanced Manufacturing Technology 101(1-4):209–221

46. Khalifa M, Barka N, Brousseau J, Bocher P (2019) Reduction of edge effect using response surface methodology and artificial neural network modeling of a spur gear treated by induction with flux concentrators, The International Journal of Advanced Manufacturing Technology, pp. 1–15

47. Barglik J, Golak S, Smalcerz A, Wieczorek T (2019) Numerical modeling of induction hardening of gear wheels made of steel AMS 6419. Metalurgija 58(1-2):143–146

48. Baldan M, Nikanorov A, Nacke B (2019) A parallel multi-fidelity optimization approach in induction hardening, COMPEL-The international journal for computation and mathematics in electrical and electronic engineering

49. Li H, Zhou W, Liu H, Li Z, He L (2021) Analysis of phase transformation and mechanical properties of 55CrMo steel during induction hardening. Journal of Testing and Evaluation 49(1)

50. Chandler H (1994) Heat treater's guide: practices and procedures for irons and steels. ASM international

51. Jamil W et al (2016) Mechanical properties and microstructures of steel panels for laminated composites in armoured vehicles. International Journal of Automotive & Mechanical Engineering 13(3)

52. Taguchi G (1986) Introduction to quality engineering: designing quality into products and processes

53. Berk J, Berk S (2000) Quality management for the technology sector. Elsevier

54. Taguchi G (1993) Taguchi on robust technology development. Bringing quality engineering upstream. ASME Press, New York

55. Roy RK (2010) A primer on the Taguchi method. Soc Manuf Eng

56. Barka N, Sattarpanah Karganroudi S, Fakir R, Thibeault P, Feujofack Kemda VB (2020) Effects of laser hardening process parameters on hardness profile of 4340 steel spline—an experimental approach. Coatings 10(4):342

57. Montgomery DC, Runger GC, Hubele NF (2009) Engineering statistics. John Wiley & Sons

58. Fowlkes WY, Creveling CM (1995) Engineering methods for robust product design: using Taguchi methods in technology and product development. Addison-Wesley

59. Grace-Martin SASK (2010) Data analysis with SPSS: a first course in applied statistics. Statistics 4:27